ACS APPLIED MATERIALS & INTERFACES

www.acsami.org Research Article

Self-Powered Filterless Narrow-Band p−n Heterojunction Photodetector for Low Background Limited Near-Infrared Image Sensor Application

Li Wang, Zhen Li, Ming Li, Shao Li, Yingchun Lu, Ning Qi, Jian Zhang,* Chao Xie, Chunyan Wu, and Lin-Bao Luo*

Cite This: *ACS Appl. Mater. Interfaces* 2020, 12, 21845−21853

Read Online

ACCESS | Metrics & More | Article Recommendations | Supporting Information

ABSTRACT: Photonic detection with narrow spectrum selectivity is very important to eliminate the signal from obtrusive light, which can improve the anti-interference ability of the infrared imaging system. While the self-driving effect inherent to the p−n junction is very attractive in optic-electronic integration, the application of the p−n junction in narrow-band photodetectors is limited by the usual broad absorption range. In this work, a self-powered filterless narrowband near-infrared photodetector based on $CuGaTe_2$/silicon p−n junction was reported. The as-fabricated photodetector exhibited typical narrow-band response which shall be ascribed to the slightly smaller band gap of Si than $CuGaTe_2$ and the restricted photocurrent generation region in the p−n heterojunction by optimizing $CuGaTe_2$ thickness. It is observed that when the thickness of $CuGaTe_2$ film is 143 nm, the device exhibits a response peak centered around 1050 nm with a full-width at half-maximum of ∼118 nm. Further device analysis reveals a specific detectivity of $\sim 10^{12}$ Jones and a responsivity of 114 mA/W under 1064 nm illumination at zero bias. It was also found that an image system based on the narrowband $CuGaTe_2$/Si photodetector showed high noise immunity for its spectral selective characteristics.

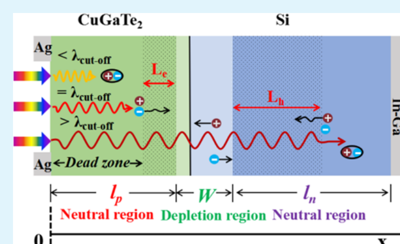

KEYWORDS: *p-n heterojunction, near infrared light, narrow band photodetector, spectral selectivity, image sensing*

Downloaded via HEFEI UNIV OF TECHNOLOGY on December 1, 2020 at 07:59:50 (UTC).
See https://pubs.acs.org/sharingguidelines for options on how to legitimately share published articles.

■ INTRODUCTION

Thanks to the capability to discriminate the infrared radiation between both target and its background, infrared (IR) imaging has demonstrated numerous applications in military and civil fields, such as security, precision guidance, process control, fire alarm, and medical care.[1−3] To improve the detection and recognition ability of the infrared system, the suppression of background disturbance is very important. As the core component of an IR imaging system, narrowband photodetector with sound spectral selectivity is of paramount importance to suppress the interference of the signal from obtrusive light. To date, narrow-band detectors have been achieved generally through using the combination of broadband photodiodes and optical filters,[4,5] bulk heterojunction based on the charge collection narrowing mechanism,[6−9] nanowire arrays,[10,11] an active layer with narrowband absorption,[12−15] and hot carrier generation with enhanced absorption in special range.[16,17] These approaches indeed can achieve photodetectors with reliable narrow band; however, these narrow band devices are usually complex in geometries, which will lead to relatively high fabrication cost, or unstable performance for their organic photo-active layers.[18,19] What is more, because these devices usually need an external power supply during operation, which means that they will consume energy in comparison with other self-driven photodetectors.

One obvious advantage of p−n junction photodetector is that it can work under zero bias, due to the photovoltaic effect.[20,21] Its spectral response should be ascribed to the superposition of responses coming from the n-type and p-type materials, respectively. While a great challenge to fabricate narrow-band photodetectors is the usual broad absorption range of the first part illuminated by light in p−n junction, few research about narrow-band detector based on p−n junction has been reported.[22] Moreover, the mechanism needs further investigation.

In recent years, chalcopyrite semiconductors Cu−III−VI_2 (III = Al, Ga, In; VI = S, Se, Te) have been extensively studied because of their potential application in solar cells and optoelectronic devices.[23−25] Among them, $CuGaTe_2$ is a typical p-type direct band gap semiconductor with high electrical conductivity and large absorption coefficient.[26−28] Its band gap is 1.18−1.40 eV, which is very close to that of silicon (1.12 eV).[29] Si-based heterojunction photodetectors have attracted significant research interest because of their

Received: February 13, 2020
Accepted: April 22, 2020
Published: April 22, 2020

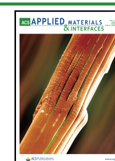

© 2020 American Chemical Society

https://dx.doi.org/10.1021/acsami.0c02827
ACS Appl. Mater. Interfaces 2020, 12, 21845−21853

excellent properties and the dominance of silicon in microelectronic technology.[30−32] Here in this study, by combining $CuGaTe_2$ with n-type Si, we achieved a sensitive self-powered narrowband near-infrared photodetector. Owing to the slightly smaller band gap than $CuGaTe_2$, Si can show highly spectral selective response to the light filtered by $CuGaTe_2$. Meanwhile, changing the thickness of $CuGaTe_2$ films can control the spectral response of the $CuGaTe_2$/silicon p−n junction in the short wavelength region by the restricted photocurrent generation region and tune the spectrum of the light shined on silicon. Device analysis revealed that the device has a response full-width at half-maximum (FWHM) of ∼118 nm, centered at around 1050 nm at zero bias, when the thickness of $CuGaTe_2$ film is about 143 nm. These results suggest that the present p−n heterostructure with a simple structure may find promising application in future optoelectronic devices as it is compatible with the microelectronic planar process based on Si.

RESULTS AND DISCUSSION

The proof-of-concept narrow band near infrared (NIR) light photodetector was basically composed of $CuGaTe_2$ nanofilms and bulk n-type Si wafers, as indicated by the schematic device structure in Figure 1a. When this device is illuminated by

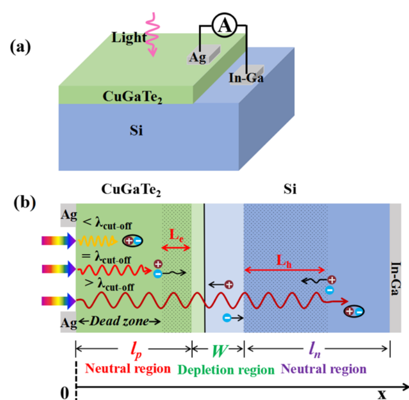

Figure 1. (a) Device structure of the $CuGaTe_2$/silicon p−n heterojunction. (b) Working principle of the as-assembled narrowband photodetector.

incident light, photo-generated free electron−hole pairs (EHPs) can be generated throughout the junction, however, only a small fraction EHPs can be converted into photogenerated current due to its unique device operation mechanism. Figure 1b shows the working principle of the present heterojunction device. The device geometry can be divided into three different regions from the silver electrode to In−Ga electrode: neutral region (l_p), depletion region (W) and neutral region (l_n). Virtually, only the EHPs in the depletion region and within a diffusion length to the depletion region of p−n junction have the opportunity to be separated and drifted by the built-in electric field, creating photocurrent. It can be seen that there is a region ($x = 0 \sim l_p - L_e$) in the first neutral region of $CuGaTe_2$ film side, which absorbs light-generating EHPs but shows no response due to recombination. This area is therefore termed as "dead-zone", which is just located in front of the photocurrent generation region in the $CuGaTe_2$/silicon p−n junction. Here, the l_p and L_e denote the thickness of the neutral region and diffusion length in the $CuGaTe_2$ nanofilm, respectively. Because of the interesting property and special position of "dead-zone", the $CuGaTe_2$/silicon p−n junction will not show any photoresponse to the light that cannot penetrate "dead-zone".

How deeply light can penetrate into a material could be described by penetration depth, which is the reciprocal of absorption coefficient α. Because EHPs are mainly generated by the photons with energy larger than semiconductor band gap, the absorption coefficient of which usually decreases with the increase of photon wavelength,[33] there should exist a critical or cutoff value for incident wavelength ($\lambda_{cut\text{-}off}$), whose penetration depth is equal to the certain "dead-zone" width. When the wavelength of the incident light is less than the $\lambda_{cut\text{-}off}$, it cannot reach the photocurrent generation region in p−n junction, because it has been absorbed completely in the "dead-zone", for its short penetration depth compared with upper $\lambda_{cut\text{-}off}$. On the contrary, it is a different story for the incident photons with wavelengths longer than the $\lambda_{cut\text{-}off}$. In this case, the photogenerated EHPs can be efficiently separated and therefore lead to the formation of photocurrent in the circuit. These discussion indicates that changing the thickness of $CuGaTe_2$ film can control not only the spectral response of $CuGaTe_2$/silicon p−n junction by defining the position of photocurrent generation region but also the spectrum of the light shined on silicon after passing through $CuGaTe_2$ nanofilm. In addition, the intensity of device responsivity is mainly determined by the thickness of the diffusion and depletion regions in p−n junction, which are correlated to carrier mobility and concentration.[34,35]

In addition, for most of semiconductor materials, their absorption coefficients usually significantly decrease when the incident wavelengths is close to wavelength ($\lambda_{band\text{-}gap}$) corresponding to their band gap.[36] As a result, the $CuGaTe_2$ nanofilm will show high transmittance to the incident light with wavelength above $\lambda_{band\text{-}gap}$. This relatively high transmittance, along with the tunable effect of $CuGaTe_2$ film thickness on the photogeneration and formation of photocurrent discussed above, suggests that the $CuGaTe_2$ film can actually act as a filter to the light shined on silicon. Because of the smaller band gap of Si than $CuGaTe_2$, incident light of wavelength ($\lambda > \lambda_{band\text{-}gap\text{-}CuGaTe2}$) is possible to excite EHPs in Si and generates photocurrent, which will make the response range of $CuGaTe_2$/Si junction wider than that obtained from $CuGaTe_2$ film alone. However considering only the photon with energy larger than the band gap of Si can excite strong photogeneration in silicon, and the very similar band gap of silicon and $CuGaTe_2$, the present $CuGaTe_2$/silicon p−n junction can achieve the narrowband light detection.

Based on the rationale outlined above, a $CuGaTe_2$ nanofilm was deposited onto an n-type Si/SiO_2 substrate with a predefined SiO_2 window, defining the effective area of the $CuGaTe_2$/silicon p−n junction, to obtain a vertical heterostructure. During the device fabrication process, pulsed laser deposition (PLD) was chosen to synthesize $CuGaTe_2$ films for the fact that it is very difficult to precisely control the chemical composition of ternary compound using other conventional thin film technology. After film deposition, Ag and In−Ga alloy were used to form Ohmic contact with $CuGaTe_2$ film and n-type silicon substrate (Figure S1, please refer to the Supporting Information for more information). A detailed device fabrication procedure can be found in the Experimental Section. Figure 2a exhibits a typical field emission scanning electron microscopy (FESEM) image of the $CuGaTe_2$ films. It shows that the film was relatively continuous and smooth,

https://dx.doi.org/10.1021/acsami.0c02827
ACS Appl. Mater. Interfaces 2020, 12, 21845−21853

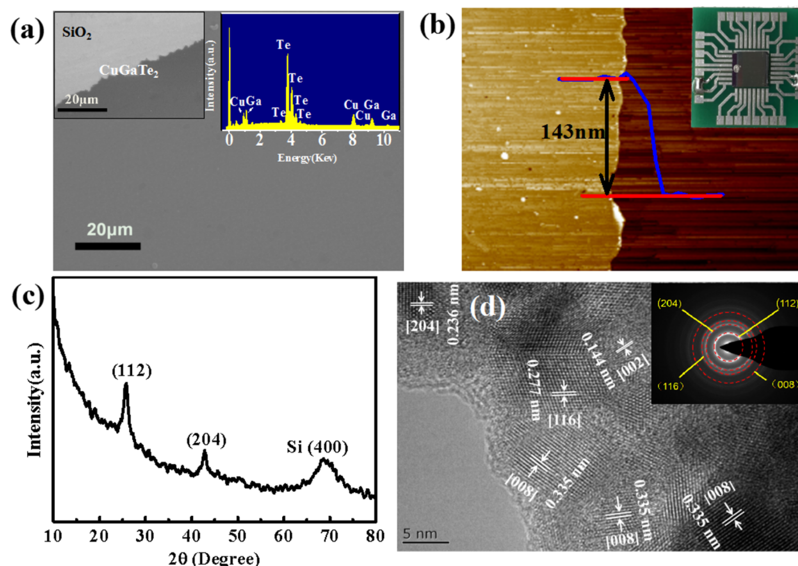

Figure 2. (a) SEM image of the $CuGaTe_2$ nanofilm with EDS analysis. The left inset shows the clear boundary between the film and the substrate. (b) AFM image of the $CuGaTe_2$ nanofilm on the Si substrate with its step height, the right inset is digital a photograph of the as-prepared photodetector. (c) XRD pattern of the $CuGaTe_2$ film. (d) HRTEM image of the $CuGaTe_2$ film with the SAED pattern.

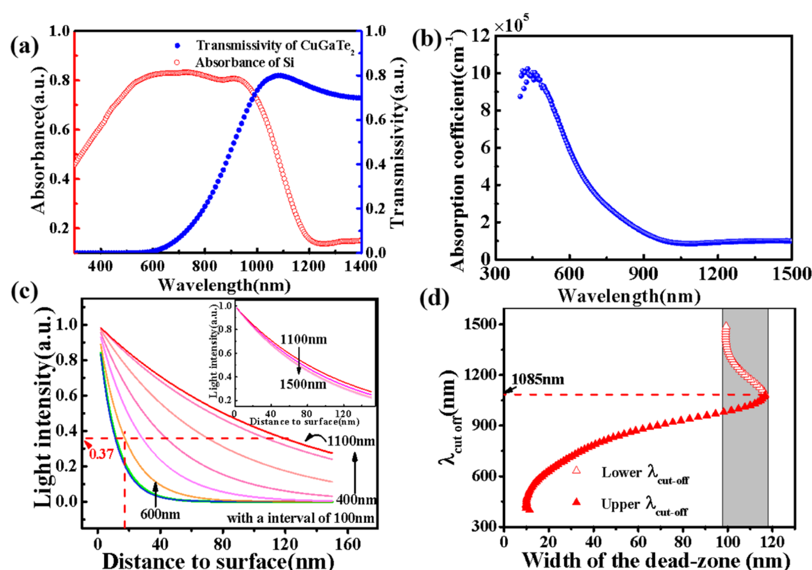

Figure 3. (a) Absorption spectrum of Si and the transmission spectrum of $CuGaTe_2$ nanofilm. (b) Absorption coefficient of $CuGaTe_2$ nanofilm. (c) Attenuation curve of the light with different wavelengths in $CuGaTe_2$ nanofilm. (d) Relationship between $\lambda_{cut\text{-}off}$ and the width of dead-zone in $CuGaTe_2$ film.

without obvious holes and large particle accumulation observed. The energy-dispersive spectroscopy (EDS) analysis of the sample revealed that the atomic ratio of Cu/Ga/Te is approximately to be 1:1:2, consistent with the composition of $CuGaTe_2$ (Table S1). What is more, the boundary of the film can be easily distinguished from SiO_2 substrate due to the difference in contrast (upper left inset in Figure 2a), which is favorable for the subsequent construction of device. The upper right inset in Figure 2b depicts the optical image of the photodetector based on $CuGaTe_2$/silicon heterojunction. The thickness of the as-prepared $CuGaTe_2$ film was about 143 nm, as shown in Figure 2b. All of the diffraction peaks in the X-ray diffraction (XRD) pattern of the PLD derived nanofilm can be assigned to $CuGaTe_2$ with a tetragonal structure (JCPDS no. 82-0446) and the (400) plane of Si substrate (Figure 2c). As a matter of fact, further characterization results including Raman study in Figure S2 and high-resolution transmission electron microscopy (HRTEM) image in Figure 2d confirm that the as-deposited sample is composed of poly-crystalline $CuGaTe_2$ films with no obvious impurity and contaminants.

Figure 3a exhibits the absorption and transmission spectra of n-type Si substrate and $CuGaTe_2$ nanofilm. There is an overlap region from 600 to 1200 nm between the two spectra, suggesting the $CuGaTe_2$ film could act as a high spectrum selectivity “window” for Si material. Specifically, the absorption coefficient of $CuGaTe_2$ is almost 10^6 cm^{-1}, for light wavelengths less than 600 nm, and decreases dramatically with the increasing wavelength (Figure 3b), as expected. Notably, the absorption coefficient nearly stop decreasing in the range from 1085 to 1500 nm. This finding is consistent

https://dx.doi.org/10.1021/acsami.0c02827
ACS Appl. Mater. Interfaces 2020, 12, 21845−21853

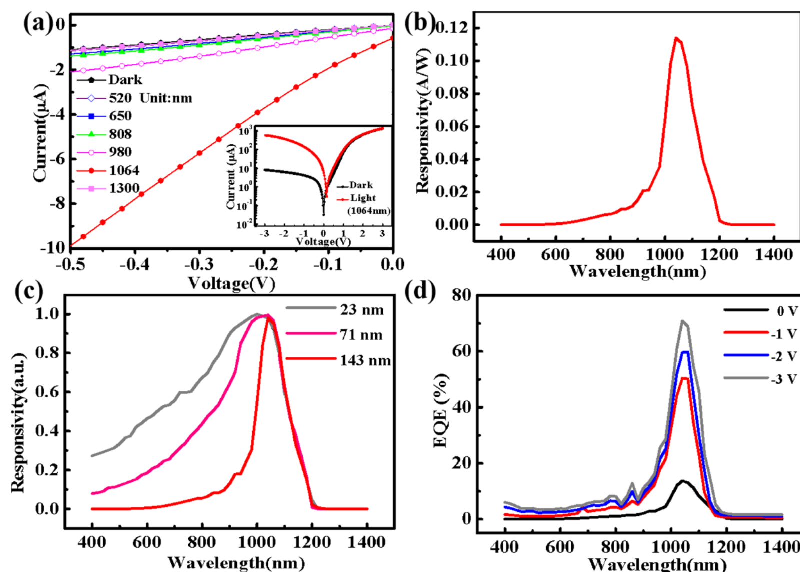

Figure 4. (a) I−V characteristics of photodetector under the light illumination of different wavelengths (1.5 mW/cm^2). The inset shows the photovoltaic behavior in semilogarithmic scale. (b) Wavelength-dependent responsivity of the device. (c) Normalized spectral responses of the photodetector with different thicknesses of $CuGaTe_2$ film. (d) EQE of the device with 143 nm $CuGaTe_2$ film under various biases of 0, −1, −2, and −3 V.

with the evolution of transmittance as a function of wavelength (Figure 3a) and can be probably related to the defects in the nanocrystalline $CuGaTe_2$ film, whose electronic levels are within the forbidden gap.[37] Figure 3c presents the attenuation curve of different wavelength light propagating in the $CuGaTe_2$ film, calculated based on the absorption coefficient results. It can be seen that the longer the wavelength of light, the slower is the decaying speed, when light wavelength is less than 1100 nm. Light of longer wavelength can penetrate into deeper position. The $CuGaTe_2$ film could almost absorb the light (<600 nm) completely, when its thickness is only about 17 nm, due to its high absorption coefficient of short wavelength. Here, light is considered to be completely absorbed when intensity decays below $1/e$ (37%) of initial value, according to the physical meaning of penetration depth.[38] Interestingly, the decaying speed of light gradually increases, as wavelength increased from 1100 to 1500 nm (photon energy below the band gap of $CuGaTe_2$), indicating a small rise of absorption coefficient in this range (inset in Figure 3c). According to the aforementioned absorption coefficient evolution as a function of light wavelength, one can anticipate that there would be a lower $\lambda_{cut\text{-}off}$ in the range of 1100−1500 nm. The light of wavelength longer than lower $\lambda_{cut\text{-}off}$ will be absorbed completely by the dead-zone, causing the penetration depth $(1/\alpha)$ of the lower $\lambda_{cut\text{-}off}$ to be equal to the width of dead-zone.

To reveal the effect of nanofilm thickness on the spectral response of p−n heterojunction device, the absorption coefficient α corresponding to the $\lambda_{cut\text{-}off}$ of various width dead-zone can be calculated according to the formula

$$\alpha = -\frac{1}{d_{\text{dead-zone}}} \ln \frac{I}{I_0} \tag{1}$$

which is derived from

$$I = I_0 \exp(-\alpha d) \tag{2}$$

where I_0, d, and $d_{\text{dead-zone}}$ are original light intensity, depth of light penetration, and dead-zone width $(I/I_0 = 1/e)$.[39] Subsequently, the value and type of $\lambda_{cut\text{-}off}$ could be deduced from Figure 3b. Figure 3d plots $\lambda_{cut\text{-}off}$ as a function of different widths of dead-zone. It is obvious that there is upper $\lambda_{cut\text{-}off}$ existed when the dead-zone width is from 0 to 120 nm, the value of which will increase with the widening of dead-zone. Allowing for the monotone decreasing tendency of absorption coefficient from 400 to 1085 nm (Figure 3b), the dead-zone in $CuGaTe_2$ will absorb the light of wavelength shorter than upper $\lambda_{cut\text{-}off}$ completely, however, without any contribution to the photocurrent. Moreover, when the width is in the range of 98−120 nm (gray area in Figure 3d), the corresponding lower $\lambda_{cut\text{-}off}$ will appear at the same time. In this range, the dead-zone will absorb the light of wavelength less than upper $\lambda_{cut\text{-}off}$ and larger than lower $\lambda_{cut\text{-}off}$ both but exhibit no response to them. It can be seen that the dead-zone width in $CuGaTe_2$ film not only control the response of $CuGaTe_2$ itself, but also tune the light incident on silicon like a filter. In a nutshell, the width of dead-zone in the $CuGaTe_2$ film is shown to be a vital factor in the narrowband detecting of $CuGaTe_2$/silicon p−n junction, which can be adjusted simply by changing the $CuGaTe_2$ film thickness.

Figure 4a depicts the I−V characteristics of $CuGaTe_2$/Si p−n heterojunction device under illumination with different wavelengths at the same light intensity (1.5 mW/cm^2). The thickness of $CuGaTe_2$ film in this device is around 143 nm. It is found that the device has displayed obvious photovoltaic characteristics when shined by 1064 nm NIR light (Figure 4a). Further comparison of the photoresponse curve finds that our device actually has apparent spectral selectivity: It shows relatively weak photoresponse to incident light with wavelengths shorter than 980 nm or longer than 1300 nm, but is very sensitive to 1064 nm light, indicating the potential applications of the device in some special optoelectronic systems that require critical wavelength selectivity. In order to further evaluate the spectral selectivity of the device in a more quantitative way, its responsivity was examined in the range from 400 to 1400 nm without any external power source. Figure 4b shows the responsivity of the heterojunction device

https://dx.doi.org/10.1021/acsami.0c02827
ACS Appl. Mater. Interfaces 2020, 12, 21845−21853

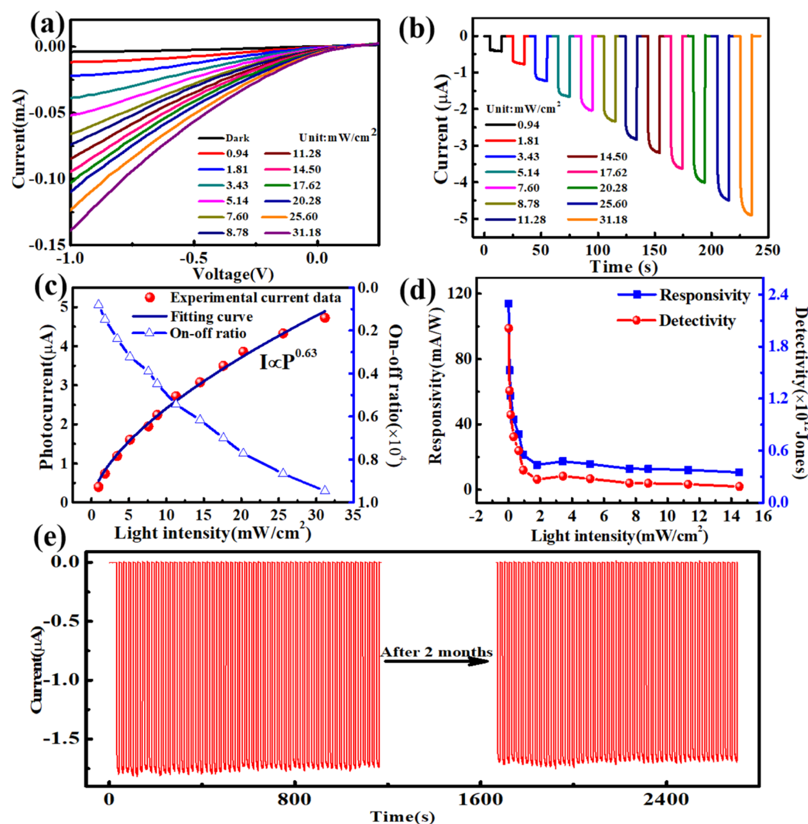

Figure 5. (a) $I-V$ curves of the heterojunction photodetector under 1064 nm light with different light intensities. (b) Time-dependent photoresponse of the device under 1064 nm light with various light intensities at zero bias. (c) On−off ratio under various light intensity and the relationship between the light intensity and photocurrent. (d) Responsivity and specific detectivity of the device as a function of incident light intensity. (e) Photoresponse of the device for 50 cycles and another 50 cycles tested after storage in air for 2 months.

in the range from 400 to 1400 nm, from which one can easily find that a peak response at 1050 nm with the FWHM about 118 nm. The device exhibited a typical narrow-band characteristic which was quite different from the spectral response of the pure $CuGaTe_2$ thin film showed in Figure S3. Moreover, when the $CuGaTe_2$ film thickness decreases, the FWHM of the $CuGaTe_2$/Si p−n heterojunction device begins to widen for the rapidly rising response of short wavelength light (Figure 4c). This trend verifies our conclusion that the $CuGaTe_2$ film thickness plays an important role in determining the spectral selectivity of $CuGaTe_2$/Si p−n heterojunction-based device.

One more thing that deserves extra discussion is that the photoresponse of the present heterojunction device actually can be further improved by applying bias voltage (Figure 4d). Taking the external quantum efficiency (EQE) for example, the EQE can be remarkably enhanced by 71% under a low negative bias of −3 V, which is about 5 times larger than that of zero bias. Meanwhile, the device can retain its narrowband detection ability within a wide range of bias voltages, with the peak position of response almost unchanged. This maybe correlated to the ultrathin depletion region in $CuGaTe_2$ film, which can be calculated according to the following formula[40]

$$W_p = \sqrt{\frac{2\varepsilon_{sp}\varepsilon_{sn}\varphi_{bi}}{qN_A\left(\varepsilon_{sn} + \frac{N_A}{N_D}\varepsilon_{sp}\right)}} \tag{3}$$

and

$$\varphi_{bi} = \frac{E_{Fn} - E_{Fp}}{q} \tag{4}$$

where ε_{sp}, ε_{sn}, N_A, N_D, E_{Fp}, and E_{Fn} are dielectric constant, impurity concentration, Fermi level of $CuGaTe_2$ and Si, q is the elementary electronic charge, and φ_{bi} is the contact potential difference between $CuGaTe_2$ and Si. The work function of the $CuGaTe_2$ film is determined to be 4.47 eV from the ultraviolet photoemission spectroscopy (UPS) measurement (Figure S4). Based on this value, the width of the depletion region in $CuGaTe_2$ is evaluated to be 0.081 nm, while that in Si is 405 nm (related parameter can be found in Table S2, please refer to the Supporting Information for more information). It can be seen that the depletion region of heterojunction was mainly in silicon. In this case, the reverse bias would effectively enhance the strength of built-in electric field in the depletion region of silicon, improving its photoelectric conversion efficiency. While the influence of bias on the depletion region in $CuGaTe_2$ could be neglected, thereby, the filtering effect and response of $CuGaTe_2$ is almost unchanged. It is shown that applying bias could be used as an effective mean to modulate the photoresponse intensity of the device (Figure S5).

In addition, the sensitivity of the present narrow-band NIR photodetector based on $CuGaTe_2$/Si p−n junction was found to greatly depend on the light intensity of the NIR illumination (Figure 5a). Figure 5b presents the time-dependent response of the device under the illuminations of 1064 nm with intensity varying from 0.94 to 31.18 mW/cm^2 at 0 V bias. For all incident intensities, the device can be readily switched between

https://dx.doi.org/10.1021/acsami.0c02827
ACS Appl. Mater. Interfaces 2020, 12, 21845−21853

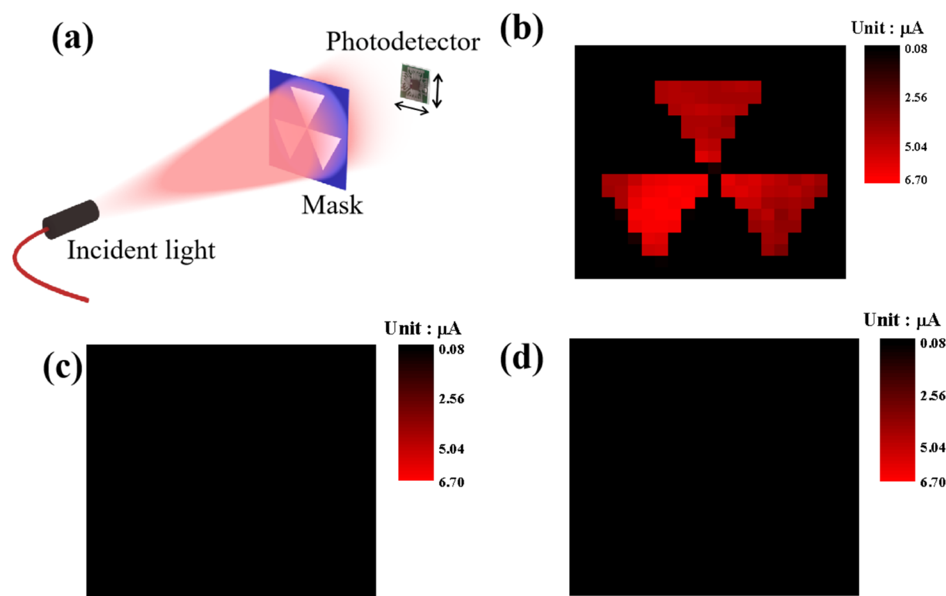

Figure 6. (a) Schematic diagram of the measurement for the image sensing study. (b−d) 2D current mapping of image sensor under 1064, 650, and 1300 nm illumination.

on-/off-states with high on−off ratio and good repeatability (Figure 5c). However, the photocurrent increases sublinearly (θ = 0.63) with the light intensity. This phenomenon could be attributed to the trap states caused by the defects in $CuGaTe_2$ film. With the increase of light intensity, the charge carriers excited by light will be filled into the defect, which leads to photocurrent saturation.[41−43] Further calculation of the device performance related parameters reveals that responsivity (R) and specific detectivity (D^*) can reach nearly 114 mA/W and 2.01 × 10^{12} Jones at light intensity of 0.026 mW/cm^2 (please refer to the Experimental Section for more information). These reasonable values of device performance indicate that photon-generated electrons and holes are effectively separated by the p−n junction and collected by respective electrodes, considering the loss of carriers caused by the filtering of $CuGaTe_2$ to achieve narrowband detection. The value of specific detectivity is even comparable to some high-performance broadband photodetectors,[44−46] showing relative strong ability of detecting weak optical signal. Furthermore, the device presented excellent repeatability and long-term durability under continuously switched 1064 nm irradiation over 50 cycles of operation (Figure 5e). It is showed that there is slight fluctuation in the response, which is probably caused by the variation of incident light. Moreover, the performance of device remained almost unchanged after 2 months' storage in air, which is understandable considering the fact that both inorganic silicon and $CuGaTe_2$ nanofilm are very stable in ambient condition.

To test the noise immunity of the image system based on the narrowband $CuGaTe_2$/Si photodetector, a lab-built mask (3 cm × 3 cm) with three open inverted triangles patterns was placed between the homogeneous illumination and the photodetector (Figure 6a). During the image sensing process, the $CuGaTe_2$/Si device will automatically collect the current of each pixel, controlled by an automatic displacement system. Meanwhile, the photocurrent of every position will be recorded and incorporated into a 2D current mapping. In this study, light sources with three different wavelengths such as 650, 1064, and 1300 nm were employed here. The area projected by illumination of 1064 nm showed photocurrent of around 5 × 10^{-6} A, while those irradiated by 650 and 1300 nm exhibited average value of 2.5 × 10^{-8} and 4.3 × 10^{-8} A, respectively. As shown in Figure 6b−d, the pattern could only be clearly identified under the irradiation of 1064 nm, implying the excellent anti-interference ability of the device to detect specific wavelength. Considering the possibility for high recognition accuracy of the present narrowband image sensor, we believe that this device shows the great potential in background limited detection.

CONCLUSIONS

In summary, a self-powered narrowband near-infrared photodetector with a central wavelength of 1050 nm has been successfully fabricated by integrating p-type $CuGaTe_2$ nanofilms with n-silicon. The experimental and theoretical calculation results showed that the thickness of $CuGaTe_2$ can tune the photocurrent generation region in p−n heterojunction, suppressing the broad absorption range of $CuGaTe_2$. Owning to similar band gap with Si, the p-type $CuGaTe_2$ film can not only form p−n junction with the n-type Si substrate but also act as a filter to the light incident on Si, controlling the spectral response of $CuGaTe_2$/silicon p−n junction. Benefited from the self-driving effect of p−n junction, the device has a responsivity (R) of 114 mA/W at zero bias, under 1064 nm light illumination. What is more, the $CuGaTe_2$/silicon heterojunction device can markedly suppress the dark current, resulting in a large on/off ratio of ∼10^4 and a high specific detectivity of ∼10^{12} Jones. The mechanism of the narrowband $CuGaTe_2$/Si photodetector can be applied to control the photoresponse of other photodetector based on p−n junction, which is very useful to improve the noise immunity of the image sensor system.

EXPERIMENTAL SECTION

Preparation and Characterization of $CuGaTe_2$ Nanofilms. $CuGaTe_2$ powders were obtained by high-energy ball milling the ingot which was prepared by a heating a mixture of high purity elemental powders (atomic ratio of Ga, Cu, and Te = 1:1:2) in an evacuated

https://dx.doi.org/10.1021/acsami.0c02827
ACS Appl. Mater. Interfaces 2020, 12, 21845−21853

quartz tube at 1273 K for 24 h with the heating rate of 2 K min^{-1}. Afterward, the target of $CuGaTe_2$ compound was fabricated by hot-pressing the prepared powder at 623 K under a pressure of 400 MPa in vacuum for 1 h. The PLD technique (Lambda Physik COMPexPro 102, 248 nm) was used to synthesize $CuGaTe_2$ films with pulsed laser power and frequency kept at 100 mJ and 3 Hz, respectively. Uniform $CuGaTe_2$ film of different thickness can be formed on the substrate at 690 K for 10−60 min under the vacuum pressure of 5×10^{-4} Pa.

The morphologies and chemical composition of the as-deposited $CuGaTe_2$ films were examined by FESEM and EDS mapping (FESEM, SIRION 200 FEG). The topography of the sample was observed using AFM (Benyuan Nanotech Com, CSPM-4000). XRD examination was performed on a Rigaku D/max-rB using Cu Kα = 1.5418 Å. The Raman spectra of samples were measured using an HR Evolution (Horiba Jobin Yvon) Raman spectrometer equipped with a 532 nm laser. The crystalline structure of the film was examined by HRTEM (FETEM, JEOL Model JEM- 2100F). The absorption spectra were tested with a UV−vis spectrophotometer (UV-2550, Shimadzu, Japan). In addition, the work function of the $CuGaTe_2$ was determined by a photoemission spectroscopy system (Thermo-VG Scientific, ESCALAB 250), in which a He lamp with 21.22 eV He I excitation energies was used.

Device Fabrication and Characterization. To construct the $CuGaTe_2$/Si heterojunction photodetector, a rectangle window (0.5 × 0.16 cm^2) was first defined on the precleaned n-type Si (1−10 Ω·cm)/SiO_2 (300 nm) substrate by photolithography. Then, the SiO_2 insulator layer within the defined area was removed by immersing the substrate into a BOE solution ($HF/NH_4F/H_2O$ = 3 mL:6 g:10 mL) for 5 min to expose the Si below. After fully removing the photoresist by acetone and cleaning, $CuGaTe_2$ films were deposited onto the substrate according to the conditions mentioned above. In−Ga alloy and Ag pastes were attached to the Si substrate and $CuGaTe_2$ film for Ohmic contact, respectively. The electrical measurement of the $CuGaTe_2$/Si photodetector was performed on a semiconductor parameter testing system (Keithley 2400). The spectral response of a detector was measured on a monochrometer (LE-SP-M300). To study the photoresponse, laser diodes with different wavelengths (HW520AL35-16GD, FU650AD5-BC9, HW808AD50-16GD, FU980AD100-BD10, ZLM50AD1064-22130BXS and M1300L3) were used as the light sources. The power intensity of all light sources was carefully calibrated using a power meter (Thorlabs GmbH., PM 100D) before measurement. All studies were conducted under ambient conditions at room temperature. The responsivity (R) was calculated as $R = \Delta I/(P{\cdot}S)$, where ΔI is the difference between the photocurrent and the dark current, P is the incident power density, and S is the effective illumination area.[47] EQE was calculated from the responsivity: $EQE = R{\cdot}h{\cdot}c/(e{\cdot}\lambda)$, where h is the Plank's constant, c is the speed of light, e is the electronic charge, and λ is the incident light wavelength.[48] The specific detectivity was calculated using the equation $D^*=(R{\cdot}S^{1/2})/(2e{\cdot}I_{dark})^{1/2}$, where I_{dark} is the dark current.[49]

ASSOCIATED CONTENT

Supporting Information

The Supporting Information is available free of charge at https://pubs.acs.org/doi/10.1021/acsami.0c02827.

> $I-V$ curves for the Ag/$CuGaTe_2$/Ag structure and In−Ga/Si/In−Ga structure, Raman spectra of the $CuGaTe_2$ film, wavelength-dependent responsivity of the $CuGaTe_2$ film (143 nm), UPS analysis, photoresponse switching behavior of the $CuGaTe_2$/silicon pn junction at varying voltages from −0.5 to −3.0 V, composition of $CuGaTe_2$ films measured with EDS, and permittivity, impurity concentration, and work function of $CuGaTe_2$ and Si (PDF)

AUTHOR INFORMATION

Corresponding Authors

Jian Zhang − *Key Laboratory of Materials Physics, Institute of Solid State Physics, Chinese Academy of Sciences, Hefei 230031, China*; orcid.org/0000-0001-6791-8949; Email: zhangjian@issp.ac.cn

Lin-Bao Luo − *School of Electronic Science and Applied Physics, Hefei University of Technology, Hefei 230009, China*; orcid.org/0000-0001-8651-8764; Email: luolb@hfut.edu.cn

Authors

Li Wang − *School of Electronic Science and Applied Physics, Hefei University of Technology, Hefei 230009, China*; orcid.org/0000-0002-9125-7447

Zhen Li − *School of Electronic Science and Applied Physics, Hefei University of Technology, Hefei 230009, China*

Ming Li − *School of Electronic Science and Applied Physics, Hefei University of Technology, Hefei 230009, China*

Shao Li − *State Key Laboratory of Metastable Materials Science & Technology, Yanshan University, Qinhuangdao 066004, China*

Yingchun Lu − *School of Electronic Science and Applied Physics, Hefei University of Technology, Hefei 230009, China*

Ning Qi − *School of Electronic Science and Applied Physics, Hefei University of Technology, Hefei 230009, China*

Chao Xie − *School of Electronic Science and Applied Physics, Hefei University of Technology, Hefei 230009, China*; orcid.org/0000-0003-4451-767X

Chunyan Wu − *School of Electronic Science and Applied Physics, Hefei University of Technology, Hefei 230009, China*

Complete contact information is available at: https://pubs.acs.org/10.1021/acsami.0c02827

Notes

The authors declare no competing financial interest.

ACKNOWLEDGMENTS

This work was supported by the National Natural Science Foundation of China (NSFC, nos. 61575059, 61675062, and 51902078), the Fundamental Research Funds for the Central Universities (JZ2018HGPB0275, JZ2018HGTA0220, JZ2018HGXC0001), and the National College Students' innovation and entrepreneurship training program (no. 201710359060).

REFERENCES

(1) Fukushima, S.; Shimatani, M.; Okuda, S.; Ogawa, S.; Kanai, Y.; Ono, T.; Matsumoto, K. High Responsivity Middle-wavelength Infrared Graphene Photodetectors Using Photo-gating. *Appl. Phys. Lett.* **2018**, *113*, 061102.

(2) Chuh, T.; Tullius, T. D. *Proceedings of the Society of Photo-Optical Instrumentation Engineers (SPIE)*; Dereniak, E. L., Sampson, R. E., Johnson, C. B., Eds.; Spie-Int Soc Optical Engineering: Bellingham, 2004; pp 19−34.

(3) Zeng, L.-H.; Wang, M.-Z.; Hu, H.; Nie, B.; Yu, Y.-Q.; Wu, C.-Y.; Wang, L.; Hu, J.-G.; Xie, C.; Liang, F.-X.; Luo, L.-B. Monolayer Graphene/Germanium Schottky Junctions as High-Performance Self-Driven Infrared Light Photodetector. *ACS Appl. Mater. Interfaces* **2013**, *5*, 9362−9366.

(4) Jansen-van Vuuren, R. D.; Armin, A.; Pandey, A. K.; Burn, P. L.; Meredith, P. Organic Photodiodes: The Future of Full Color Detection and Image Sensing. *Adv. Mater.* **2016**, *28*, 4766−4802.

(5) Yokogawa, S.; Burgos, S. P.; Atwater, H. A. Plasmonic Color Filters for CMOS Image Sensor Applications. *Nano Lett.* **2012**, *12*, 4349−4354.
(6) Rao, H.-S.; Li, W.-G.; Chen, B.-X.; Kuang, D.-B.; Su, C.-Y. In Situ Growth of 120 cm^2 $CH_3NH_3PbBr_3$ Perovskite Crystal Film on FTO Glass for Narrowband-Photodetectors. *Adv. Mater.* **2017**, *29*, 1602639.
(7) Lin, Q.; Armin, A.; Burn, P. L.; Meredith, P. Filterless Narrowband Visible Photodetectors. *Nat. Photonics* **2015**, *9*, 687−694.
(8) Fang, Y.; Dong, Q.; Shao, Y.; Yuan, Y.; Huang, J. Highly Narrowband Perovskite Single-Crystal Photodetectors Enabled by Surface-Charge Recombination. *Nat. Photonics* **2015**, *9*, 679−686.
(9) Armin, A.; Vuuren, R. D. J. V.; Kopidakis, N.; Burn, P. L.; Meredith, P. Narrowband Light Detection via Internal Quantum Efficiency Manipulation of Organic Photodiodes. *Nat. Commun.* **2015**, *6*, 6343.
(10) Solanki, A.; Li, S.; Park, H.; Crozier, K. B. Harnessing the Interplay between Photonic Resonances and Carrier Extraction for Narrowband Germanium Nanowire Photodetectors Spanning the Visible to Infrared. *ACS Photonics* **2018**, *5*, 520−527.
(11) Crozier, K. B.; Seo, K.; Park, H.; Solanki, A.; Li, S. Q. Controlling the Light Absorption in a Photodetector Via Nanowire Waveguide Resonances for Multispectral and Color Imaging. *IEEE J. Sel. Top. Quantum Electron.* **2018**, *24*, 1.
(12) Xiong, Q.; Chowdhury, F. I.; Wang, X. Filter-Free Narrowband Photodetectors Employing Colloidal Quantum Dots. *IEEE J. Sel. Top. Quantum Electron.* **2018**, *24*, 1.
(13) Yoon, S.; Ha, Y.-H.; Kwon, S.-K.; Kim, Y.-H.; Chung, D. S. Fabrication of High Performance, Narrowband Blue-Selective Polymer Photodiodes with Dialkoxynaphthalene-Based Conjugated Polymer. *ACS Photonics* **2018**, *5*, 636−641.
(14) Lee, K.-H.; Lee, G. H.; Leem, D.-S.; Lee, J.; Chung, J. W.; Bulliard, X.; Choi, H.; Park, K.-B.; Kim, K.-S.; Jin, Y. W.; Lee, S.; Park, S. Y. Dynamic Characterization of Green-Sensitive Organic Photodetectors Using Nonfullerene Small Molecules: Frequency Response Based on the Molecular Structure. *J. Phys. Chem. C* **2014**, *118*, 13424−13431.
(15) Li, J.; Wang, J.; Ma, J.; Shen, H.; Li, L.; Duan, X.; Li, D. Self-Trapped State Enabled Filterless Narrowband Photodetections in 2D Layered Perovskite Single Crystals. *Nat. Commun.* **2019**, *10*, 806.
(16) Tanzid, M.; Ahmadivand, A.; Zhang, R.; Cerjan, B.; Sobhani, A.; Yazdi, S.; Nordlander, P.; Halas, N. J. Combining Plasmonic Hot Carrier Generation with Free Carrier Absorption for High-Performance Near-Infrared Silicon-Based Photodetection. *ACS Photonics* **2018**, *5*, 3472−3477.
(17) Sobhani, A.; Knight, M. W.; Wang, Y.; Zheng, B.; King, N. S.; Brown, L. V.; Fang, Z.; Nordlander, P.; Halas, N. J. Narrowband Photodetection in the Near-Infrared with a Plasmon-Induced Hot Electron Device. *Nat. Commun.* **2013**, *4*, 1643.
(18) Miao, J.; Zhang, F.; Du, M.; Wang, W.; Fang, Y. Photomultiplication Type Narrowband Organic Photodetectors Working at Forward and Reverse Bias. *Phys. Chem. Chem. Phys.* **2017**, *19*, 14424−14430.
(19) Periyanagounder, D.; Wei, T. C.; Li, T. Y.; Lin, C. H.; Gonçalves, T. P.; Fu, H. C.; Tsai, D. S.; Ke, J. J.; Kuo, H. W.; Huang, K. W.; Lu, N.; Fang, X.; He, J. H. Fast-Response, Highly Air-Stable, and Water-Resistant Organic Photodetectors Based on a Single-Crystal Pt Complex. *Adv. Mater.* **2020**, *32*, 1904634.
(20) Wu, D.; Guo, J.; Du, J.; Xia, C.; Zeng, L.; Tian, Y.; Shi, Z.; Tian, Y.; Li, X. J.; Tsang, Y. H.; Jie, J. Highly Polarization-Sensitive, Broadband, Self-Powered Photodetector Based on Graphene/$PdSe_2$/Germanium Heterojunction. *ACS Nano* **2019**, *13*, 9907−9917.
(21) Lu, Z.; Xu, Y.; Yu, Y.; Xu, K.; Mao, J.; Xu, G.; Ma, Y.; Wu, D.; Jie, J. Ultrahigh Speed and Broadband Few-Layer MoTe2/Si 2-3D Heterojunction-Based Photodiodes Fabricated by Pulsed Laser Deposition. *Adv. Funct. Mater.* **2020**, *30*, 1907951.
(22) Zhu, H.; Shan, C. X.; Yao, B.; Li, B. H.; Zhang, J. Y.; Zhao, D. X.; Shen, D. Z.; Fan, X. W. High Spectrum Selectivity Ultraviolet Photodetector Fabricated from an n-ZnO/p-GaN Hetero junction. *J. Phys. Chem. C* **2008**, *112*, 20546−20548.
(23) Welch, A. W.; Baranowski, L. L.; Peng, H.; Hempel, H.; Eichberger, R.; Unold, T.; Lany, S.; Wolden, C.; Zakutayev, A. Trade-Offs in Thin Film Solar Cells with Layered Chalcostibite Photovoltaic Absorbers. *Adv. Energy Mater.* **2017**, *7*, 1601935.
(24) Lu, P.; Li, R.; Yao, N.; Dai, X.; Ye, Z.; Zheng, K.; Kong, W.; Fang, W.; Li, S.; Xu, Q.; Wu, H. Enhancement of Two-Photon Fluorescence and Low Threshold Amplification of Spontaneous Emission of Zn-processed $CuInS_2$ Quantum Dots. *ACS Photonics* **2018**, *5*, 1310−1317.
(25) Abou-Ras, D.; Bär, M.; Caballero, R.; Gunder, R.; Hages, C.; Heinemann, M. D.; Kaufmann, C. A.; Krause, M.; Levcenko, S.; Mainz, R.; Márquez, J.; Nikolaeva, A.; Redinger, A.; Schäfer, N.; Schorr, S.; Stange, H.; Unold, T.; Wilks, R. G. Advanced Characterization and In-Situ Growth Monitoring of Cu(In,Ga)Se2 Thin Films and Solar Cells. *Solar Energy* **2018**, *170*, 102−112.
(26) Plirdpring, T.; Kurosaki, K.; Kosuga, A.; Day, T.; Firdosy, S.; Ravi, V.; Snyder, G. J.; Harnwunggmoung, A.; Sugahara, T.; Ohishi, Y.; Muta, H.; Yamanaka, S. Chalcopyrite $CuGaTe_2$: A High-Efficiency Bulk Thermoelectric Material. *Adv. Mater.* **2012**, *24*, 3622−3626.
(27) Zhang, J.; Huang, L.; Zhu, C.; Zhou, C.; Jabar, B.; Li, J.; Zhu, X.; Wang, L.; Song, C.; Xin, H.; Li, D.; Qin, X. Design of Domain Structure and Realization of Ultralow Thermal Conductivity for Record-High Thermoelectric Performance in Chalcopyrite. *Adv. Mater.* **2019**, *31*, 1905210.
(28) Abd El-hady, S. A.; Mansour, B. A.; Moustafa, S. H. Growth and Spectral Dependence of the Absorption Coefficient of $CuGaTe_2$ Thin Films. *Phys. Status Solidi A* **1995**, *149*, 601−609.
(29) Gombia, E.; Leccabue, F.; Pelosi, C.; Seuret, D. Vapor Growth, Thermodynamical Study and Characterization of CulnTe $_2$ and $CuGaTe_2$ Single Crystals. *J. Cryst. Growth* **1983**, *65*, 391−396.
(30) Zheng, Z.; Yao, J.; Wang, B.; Yang, Y.; Yang, G.; Li, J. Self-Assembly High- Performance UV−vis−NIR Broadband β-In_2Se_3/Si Photodetector Array for Weak Signal Detection. *ACS Appl. Mater. Interfaces* **2017**, *9*, 43830−43837.
(31) Gao, W.; Zheng, Z.; Huang, L.; Yao, J.; Zhao, Y.; Xiao, Y.; Li, J. Self-Powered $SnS_{1-x}Se_x$ Alloy/Silicon Heterojunction Photodetectors with High Sensitivity in a Wide Spectral Range. *ACS Appl. Mater. Interfaces* **2019**, *11*, 40222−40231.
(32) Flemban, T. H.; Haque, M. A.; Ajia, I.; Alwadai, N.; Mitra, S.; Wu, T.; Roqan, I. S. A Photodetector Based on p-Si/n-ZnO Nanotube Heterojunctions with High Ultraviolet Responsivity. *ACS Appl. Mater. Interfaces* **2017**, *9*, 37120−37127.
(33) Green, M. A.; Ho-Baillie, A.; Snaith, H. J. The Emergence of Perovskite Solar Cells. *Nat. Photonics* **2014**, *8*, 506−514.
(34) Ostroverkhova, O. *Handbook of Organic Materials for Electronic and Photonic Devices*; Woodhead Publishing: Oxford, 2019; p 224.
(35) Sze, S. M.; Ng, K. K. *Physics of Semiconductor Devices*; John Wiley & Sons: New York, 2006; p 81.
(36) Rogalski, A. *Infrared Detectors*; Gordon and Breach Science Publishers: Amsterdam, 2000; p 32.
(37) Grundmann, M. *The Physics of Semiconductors*; Springer-Verlag: Berlin, 2010; p 193.
(38) Ye, L. X. *The Physics of Semiconductors*; Higher Education Press: Beijing, 2004; p 502.
(39) Grundmann, M. *The Physics of Semiconductors*; Springer-Verlag: Berlin, 2010; p 268.
(40) Sze, S. M.; Ng, K. K. *Physics of Semiconductor Devices*; John Wiley & Sons: New York, 2006; p 89.
(41) Zhou, X.; Gan, L.; Tian, W.; Zhang, Q.; Jin, S.; Li, H.; Bando, Y.; Golberg, D.; Zhai, T. Ultrathin $SnSe_2$ Flakes Grown by Chemical Vapor Deposition for High-Performance Photodetectors. *Adv. Mater.* **2015**, *27*, 8035−8041.
(42) Zhao, H.; Zhang, Y.; Li, T.; Li, Q.; Yu, Y.; Chen, Z.; Li, Y.; Yao, J. Self-Driven Visible-Near Infrared Photodetector with Vertical $CsPbBr_3$/PbS Quantum Dots Heterojunction Structure. *Nanotechnology* **2020**, *31*, 035202.

https://dx.doi.org/10.1021/acsami.0c02827
ACS Appl. Mater. Interfaces 2020, 12, 21845−21853

(43) Wang, L.; Jie, J.; Shao, Z.; Zhang, Q.; Zhang, X.; Wang, Y.; Sun, Z.; Lee, S.-T. MoS_2/Si Heterojunction with Vertically Standing Layered Structure for Ultrafast, High-Detectivity, Self-Driven Visible−Near Infrared Photodetectors. *Adv. Funct. Mater.* **2015**, *25*, 2910−2919.
(44) Alwadai, N.; Haque, M. A.; Mitra, S.; Flemban, T.; Pak, Y.; Wu, T.; Roqan, I. High-Performance Ultraviolet-to-Infrared Broadband Perovskite Photodetectors Achieved via Inter-/Intraband Transitions. *ACS Appl. Mater. Interfaces* **2017**, *9*, 37832−37838.
(45) Liu, J.-Q.; Gao, Y.; Wu, G.-A.; Tong, X.-W.; Xie, C.; Luo, L.-B.; Liang, L.; Wu, Y.-C. Silicon/Perovskite Core−Shell Heterojunctions with Light-Trapping Effect for Sensitive Self-Driven Near-Infrared Photodetectors. *ACS Appl. Mater. Interfaces* **2018**, *10*, 27850−27857.
(46) Shin, G. H.; Park, J.; Lee, K. J.; Lee, G.-B.; Jeon, H. B.; Choi, Y.-K.; Yu, K.; Choi, S.-Y. Si−MoS_2 Vertical Heterojunction for a Photodetector with High Responsivity and Low Noise Equivalent Power. *ACS Appl. Mater. Interfaces* **2019**, *11*, 7626−7634.
(47) Saidaminov, M. I.; Haque, M. A.; Savoie, M.; Abdelhady, A. L.; Cho, N.; Dursun, I.; Buttner, U.; Alarousu, E.; Wu, T.; Bakr, O. M. Perovskite Photodetectors Operating in Both Narrowband and Broadband Regimes. *Adv. Mater.* **2016**, *28*, 8144−8149.
(48) Hu, L.; Yan, J.; Liao, M.; Wu, L.; Fang, X. Ultrahigh External Quantum Efficiency from Thin SnO_2 Nanowire Ultraviolet Photodetectors. *Small* **2011**, *7*, 1012−1017.
(49) Shao, Z. B.; Jiang, T. H.; Zhang, X. J.; Zhang, X. H.; Wu, X. F.; Xia, F. F.; Xiong, S. Y.; Lee, S. T.; Jie, J. S. Memory Phototransistors Based on Exponential-Association Photoelectric Conversion Law. *Nat. Commun.* **2019**, *10*, 1294.

https://dx.doi.org/10.1021/acsami.0c02827
ACS Appl. Mater. Interfaces 2020, 12, 21845−21853